Formation of an r8-Dominant Si Material

S. Wong,[1,7] B. Haberl,[2] B. C. Johnson,[3] A. Mujica,[4] M. Guthrie,[5,6] J. C. McCallum,[3] J. S. Williams,[1] and J. E. Bradby[1]
[1]*Department of Electronic Materials Engineering, Research School of Physics and Engineering, The Australian National University, Canberra, Australian Capital Territory 0200, Australia*
[2]*Neutron Sciences Directorate, Oak Ridge National Laboratory, Neutron Scattering Division, Oak Ridge, Tennessee 37781, USA*
[3]*School of Physics, The University of Melbourne, Melbourne, Victoria 3010, Australia*
[4]*Departamento de Fisica, MALTA Consolider Team, Universidad de La Laguna, La Laguna 38206, Tenerife, Spain*
[5]*European Spallation Source, Lund, SE-221 00, Sweden*
[6]*School of Physics, University of Edinburgh, Edinburgh, EH9 3FD, United Kingdom*
[7]*Department of Physics, School of Science, RMIT University, Victoria 3001, Australia*

(Received 1 November 2018; published 11 March 2019)

The rhombohedral phase of Si (r8-Si), a promising semiconducting material, is formed by indentation together with the body-centered cubic phase (bc8-Si). Using a novel sample preparation method, x-ray diffraction is used to determine the relative volume of these phases in indented Si and allow observation of a distorted unit cell along the direction of indentation loading. Theoretical calculations together with these observations suggest the indent contains an intrinsic compression of ~4 GPa that stabilizes the r8 phase.

DOI: 10.1103/PhysRevLett.122.105701

Silicon undergoes a series of polymorphic phase transformations under the application of high pressure [1–7]. Each phase has unique optical and electrical properties and several, being stable under ambient conditions, may be used for future device applications [8–13]. A clear advantage is that these materials can be easily integrated into standard Si as well as its processing protocols and device structures by localized pressure application. The rhombohedral phase of Si (r8-Si) is a promising semiconducting material predicted to have a narrower band gap than the standard diamond cubic phase (dc-Si) [14]. r8-Si is also predicted to have a substantially increased optical absorption over the solar spectrum range compared to dc-Si, making it particularly attractive for use in Si-based photovoltaic devices [15,16].

The r8-Si phase can be obtained with a diamond anvil cell (DAC) or indentation. In DAC compression of Si, dc-Si transforms to the white tin phase, (β-Sn)-Si, at a critical pressure of ~11 GPa [7,17]. Upon decompression, the β-Sn phase transforms to r8-Si at ~9 GPa. In a DAC, this r8 phase is not stable at ambient conditions but further transforms to the body-centered cubic phase (bc8-Si) at ~2 GPa [18]. Minimal amounts of r8-Si have been recovered after DAC decompression [6]. In contrast, under local pressure application using indentation, the persistence of r8-Si has been widely reported, alongside bc8-Si, after complete pressure unloading [3,19–21]. The electrical properties of the bc8/r8 material made by indentation have been determined to be advantageous for semiconductor applications aligned with the above predictions [22]. These properties were only explainable through the presence of a significant fraction of r8-Si. However, the mechanism for this persistent stability of r8-Si is not known, nor is there any detailed knowledge about this bc8/r8 composite material, its relative fraction, or structure. Indeed, there remains some controversy as to whether r8-Si is even obtained after unloading given the general absence of r8-Si in DAC experiments and the expected similarity between the Raman spectra of bc8-Si and r8-Si [22].

Here, we show the results of a direct x-ray diffraction (XRD) study on the small regions of material phase transformed via indentation using a novel approach, whereby a dense array of indented material is produced and probed. We demonstrate that indentation of a Si surface results in a predominantly r8-Si composite material. Furthermore, the unique structure of the indentation-induced transformation is shown to provide the conditions for r8-Si to remain stable upon unloading and thus recoverable for potential applications.

XRD is commonly used for characterization of crystalline structures, including determining phase fractions within a composite material [23]. However, no XRD results have been previously reported on the metastable Si phases made by indentation due to the difficulty in measuring sufficient signal from a single indented region (~50 μm^3 per indent for large indenter tips [24]) to allow for Rietveld refinement. Here, this limitation is overcome by employing a novel sample preparation method that forms a close-packed array of indents imbedded into a relaxed amorphous Si (a-Si) layer [see Fig. 1(a)] to drastically increase the amount of material probed. A relaxed a-Si layer was chosen as it is known to transform structurally to the bc8/r8 composite under indentation pressure in a manner similar to dc-Si [25] while avoiding the negative factors that

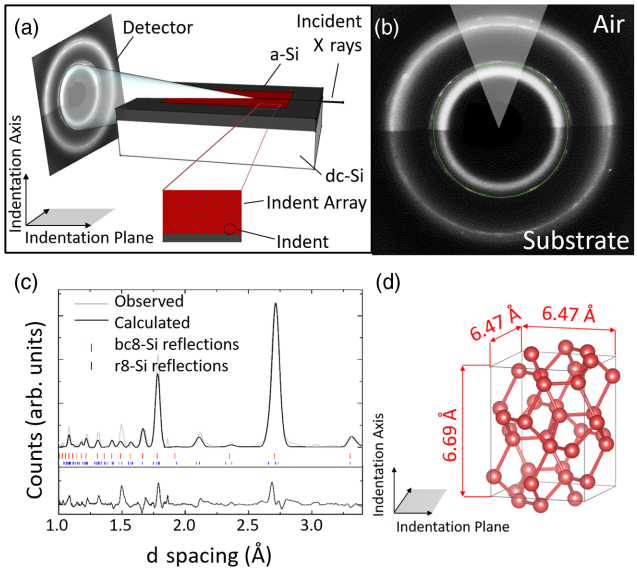

FIG. 1. (a) Schematic of the close-packed array of indents in a layer of a-Si, which allows the incident x rays to probe a sufficient volume of the bc8/r8 composite for XRD analysis (see Supplemental Material Fig. S3 for SEM). (b) XRD image of the bc8/r8 composite alongside the a-Si signal from the substrate. The image appears as if divided horizontally since the x rays are attenuated when traversing the sample. (c) Rietveld refinement of the integrated profile from the conical region indicated in (b), which is composed of x rays that have diffracted normal to the sample surface. The ticks show the positions of the bc8-Si (red) and r8-Si (blue) reflections based on the unit cell parameters calculated via refinement. The residual profile has been included below and shares the same y axis scale as the profile. (d) Schematic of an elongated bc8-Si unit cell aligned along the indentation axis.

are present for a crystalline substrate (e.g., crystalline defects forming instead of phase transformation [24,26] or a strong crystalline background signal in XRD).

A dc-Si sample was self-ion implanted with Si ions to form a 2 μm thick layer of a-Si, followed by annealing at 450 °C for 30 min to relax the a-Si layer [27]. An 80×10 array of indentations, with 10 μm separation, was performed on this layer using a 30 μm radius spherical tip to a maximum load of 700 mN with an unloading rate of 10 mN/s, resulting in a transformed region 10 μm in diameter. These conditions were chosen to maximize the volume of bc8/r8 material recovered from each indent [28]. The presence of the bc8/r8 composite after indentation was confirmed using the load-unload curve (see Supplemental Material Fig. S1 [29]) and Raman microspectroscopy [see Fig. 2(c) and Supplemental Material Fig. S2]. XRD data were taken on the 34-ID-E beamline at the Advanced Photon Source (Argonne National Laboratory) using a 24.5 keV incident beam with a Dectris Pilatus detector. The incident beam was chosen such that no signal from the underlying dc-Si substrate was detected. Diffraction patterns were integrated using Dioptas

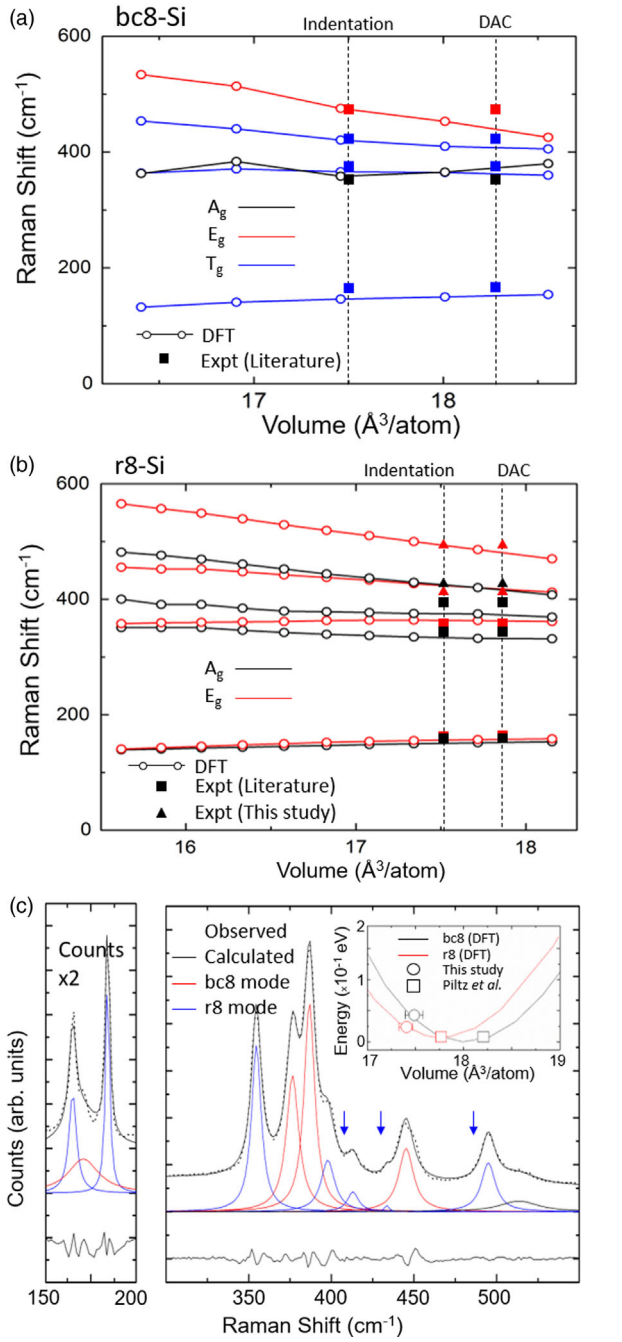

FIG. 2. Plots of the DFT-calculated Raman peak shift of (a) bc8-Si and (b) r8-Si with respect to the volume per atom. The A_g, E_g, and T_g phonon modes are indicated in black, red, and blue, respectively. The vertical lines indicate the volume of the recovered phase after indentation (as reported in this study) and DAC compression (from Ref. [6]). The experimentally observed peak positions from Ref. [33] (squares) and this study (triangles) have been indicated for both volumes. (c) Fitted Raman spectrum taken from the bc8/r8 composite. Three peaks that were not previously reported but are predicted by DFT calculations can be observed (blue arrows). (Inset) Plot of the calculated energy as a function of the volume per atom for the bc8 and r8 phases. The experimentally observed volume of the bc8 and r8 phases after indentation and DAC compression are indicated.

[34], and Rietveld refinements of the integrated profiles were performed using GSAS-II [35]. While Raman spectroscopy revealed relative peak intensity variations across the indentation zone, the XRD samples the entire array, giving an average phase fraction.

XRD results are shown in Fig. 1(b). The XRD image is divided horizontally, with the top brighter than the bottom half. This is due to the grazing angle of the incident beam, resulting in half of the diffracted signal being attenuated by the sample. Both broad rings associated with the *a*-Si substrate and spotty rings associated with the polycrystalline bc8/r8 composite can be observed. Closer inspection of the rings associated with the composite indicates a horizontal elongation. Elongation is only observed in the rings associated with the bc8/r8 composite and not the *a*-Si, indicating that this distortion is due to the indentation process rather than an artefact of the measurement. The elongation of these rings will be discussed in more detail below. For Rietveld refinement, it is only necessary to note that the elongation results in peak broadening, which obscures detail. To minimize the broadening, diffraction profiles were integrated over a conical region (~60° arc) rather than across the entire image. Furthermore, to minimize any variance introduced by conical region selection, several regions were used for profile integration. Figure 1(c) shows Rietveld refinement of an integrated profile formed from the conical region indicated in Fig. 1(b) (see Supplemental Material Fig. S4 for refinement of profiles formed across different regions). The tick marks show the positions of the allowed reflections for bc8-Si (red) and r8-Si (blue) determined by the refinement. Refinements were also attempted using only bc8-Si or only r8-Si (see Supplemental Material Fig. S5) but no satisfactory fit was achieved, indicating that the measured profile cannot be accounted for by solely one phase. The average r8-Si phase fraction across all integrated profiles is $70 \pm 10\%$ of the total material.

The elongation of the rings within the XRD image suggests a larger diffraction angle (i.e., smaller lattice spacing) for photons diffracted along the sample surface from the same (*hkl*) planes. The unit cell parameters extracted from the refinements, separated between those from vertical regions (diffracted along the sample normal) and horizontal regions (diffracted along the sample plane), are presented in Table I alongside the reported parameters from DAC experiments [6]. The unit cell lengths calculated along the sample normal in this work are significantly larger than those reported from DAC experiments, while the opposite is true along the sample plane. Therefore, the crystallites of bc8-Si and r8-Si recovered after indentation possess distorted unit cells that have a tensile strain along the sample normal and compressive strain perpendicular to it, with respect to the same phases obtained through quasihydrostatic conditions using conventional DAC.

A refined volume can be calculated for this distorted unit cell. As the recovered crystallites are randomly orientated, a distortion along the indentation axis results in many differently distorted unit cell shapes. For ease of calculation, consider a bc8-Si unit cell that is aligned along the indentation axis, i.e., a nominally cubic structure that has been elongated into a tetragonal structure such as the schematic shown in Fig. 1(d). This elongated structure has a unit length of 6.67 Å normal to the surface, a length of 6.46 Å along the other two axes, and thus a volume of 280 ± 2 Å, which is ~4% smaller than the volume of bc8-Si recovered from a DAC (292 Å). To verify the unit cell distortion and the resulting volume reduction of the bc8-Si unit cell, electron diffraction was performed (see Supplemental Material Fig. S6 for details [36]). A similar unit cell distortion was observed and a volume of 282 ± 1 Å was measured, which is in excellent agreement with the XRD observations. A similar volume calculation can be performed using the r8-Si unit cell parameters observed via XRD, resulting in a volume of 138.5 ± 1 Å.

TABLE I. Average unit cell parameters of bc8-Si and r8-Si obtained upon refinement on a region composed of photons diffracted along the indentation (Ind.) axis and plane. The parameters from bc8-Si and r8-Si recovered after DAC compression from Ref. [6] are listed for comparison. Results indicate a unit cell that is elongated in the indentation axis and compressed in the indentation plane.

	Ind. Axis	Ind. Plane	Piltz *et al.* [6]
a_{bc8} (Å)	6.69 ± 0.02	6.47 ± 0.02	6.64 ± 0.01
a_{r8} (Å)	5.82 ± 0.03	5.62 ± 0.02	5.739 ± 0.01
α_{r8} (°)	109.95 ± 0.1	110.08 ± 0.1	109.99 ± 0.1

These reduced volumes can be correlated with bc8-Si or r8-Si under hydrostatic compression. The equivalent amount of compression required to cause a similar reduction in volume can be calculated using the Birch-Murnaghan equation of state [37]. Using the values published by Piltz *et al.* [6] for the bulk modulus and its pressure derivative ($B_0 = 120$ GPa, $B_0' = 5$ GPa), the change in volume is equivalent to a compression of ~4 GPa. For r8-Si, using an initial volume of 143.5 Å^3, $B_0 = 96$ GPa, and $B_0' = 5$ GPa [6], the change in volume is likewise equivalent to ~4 GPa of compression. We propose that this reduction in volume is related to the source of residual stress that allows a significant amount of r8-Si to persist upon complete load release.

To shed further light on the nature of the recovered bc8/r8 mixture, Raman spectroscopy and theoretical calculations were carried out and compared. Raman microscopy was performed using the 532 nm line of a frequency doubled Nd:YAG laser. Theoretical calculations of the total energy and lattice dynamics of the two phases were performed within the *ab initio* framework of the density functional theory (DFT), using the pseudopotential and plane waves method of calculation, as implemented in the

VASP code [38,39]. The generalized gradient approximation was adopted for the exchange-correlation functional [40] as well as the projector augmented wave scheme [41], with other details of the calculation similar to those in Ref. [42]. The Raman peak positions of bc8-Si and r8-Si were calculated as a function of volume to determine if a smaller unit cell volume results in a closer agreement to the experimental Raman data.

Figures 2(a) and 2(b) show the calculated Raman peak positions of the bc8-Si and r8-Si phases, respectively, as a function of volume per atom. The peaks are color coded according to their assigned phonon mode, with black, red, and blue lines corresponding to A_g, E_g, and T_g modes, respectively. The volume per atom for phases recovered after DAC compression as reported in the literature (V_{DAC}), and after indentation as presented here (V_{ind}), are indicated by vertical lines. The peak positions experimentally reported in previous experiments [33,43,44] at both V_{DAC} and V_{ind} are indicated by squares, with these particular phonon mode assignments taken from Johnson *et al.* [33]. An exception is made for the bc8-Si peak at 437.5 cm^{-1}, which we believe was erroneously assigned to the E_u phonon mode. It is assigned to the T_g mode here, which is in much closer agreement to the calculated DFT data.

For the calculated Raman modes of bc8-Si presented in Fig. 2(a), there is close agreement between observed and calculated peak positions of the main peak at ~435 cm^{-1} and the peak at ~465 cm^{-1} at V_{ind}. Furthermore, there is a significant improvement in the agreement when compared to the agreement at V_{DAC}. The positions of the two peaks around ~380 cm^{-1} were not calculated to vary significantly with changing volume, thus no substantial improvement is observed when comparing the two agreements. However, the experimentally reported peak positions indicate that the T_g peak has a larger Raman shift than the A_g peak. This is in agreement with the calculated positions at V_{ind}, but not at V_{DAC}. For the calculated Raman modes of r8-Si presented in Fig. 2(b), several of the Raman peaks predicted by the DFT study in the 400–500 cm^{-1} range have not been previously reported. Figure 2(c) shows a fitted Raman spectrum taken from a bc8/r8 composite recovered after indentation, with the peaks attributed to r8-Si indicated in blue. For the previously reported r8-Si peaks, all are observed within this spectrum at their reported peak positions [33]. Additional peaks (indicated by the blue arrows) were also observed at 413, 433, and 495 cm^{-1}. The positions of these additional peaks have been included in Fig. 2(b) as indicated by the triangles. For the peaks in the <430 cm^{-1} range (165, 170, 352, 373, 397, and 413 cm^{-1}), there is a rough agreement between the observed and calculated peak positions both when considering V_{ind} and V_{DAC}. However, the peaks observed at 433 and 495 cm^{-1} are in strong agreement with the calculated peak positions at V_{ind}, which is an improvement over the agreement at V_{DAC}. The improvement in agreement between the experimentally observed and DFT-calculated Raman peak positions at V_{ind}, compared to at V_{DAC}, provides strong evidence for the presence of volume reduction due to unit cell distortion, as observed here using XRD and electron diffraction. Beyond the agreement with an indentation-induced bc8/r8 composite, the simulated shifts in peak position with varying volume and pressure are also consistent with observed shifts during decompression of expanded-volume clathrates [45] that the authors of Ref. [45] speculated are due to the formation of a bc8/r8 composite, a possibility to which our present results lend support.

The inset in Fig. 2(c) plots the energy of each phase as a function of volume per atom with the points from DAC and indentation indicated. The volumes of the bc8-Si and r8-Si recovered after DAC compression correspond to the lowest energy state possible. Conversely, the phases in the bc8/r8 composite observed in this study have different energies but have a common volume. This suggests that the bc8-Si and r8-Si within the composite material converges to a common volume rather than to the lowest energy state of each respective phase. This common volume results in a much smaller volume difference from the DAC case for r8-Si compared with bc8-Si. Interestingly, r8-Si is the energetically favored phase at this reduced volume. We propose that this is the origin of the significant amounts of r8-Si that can be recovered after complete indentation load removal.

This observed reduction in unit cell volume also reconciles the seemingly contradictory reports between r8-Si obtained after indentation and r8-Si obtained during DAC compression. One such inconsistency is that the residual stress within the bc8/r8 composite, calculated using Raman peak shift to be 0.4 GPa, is too low for the r8 phase to remain stable [46]. This residual stress value of 0.4 GPa is calculated using the Raman shift observed in the main dc-Si peak at ~520 cm^{-1} [47] and not directly from the transformed region. Here, using data collected directly from the bc8/r8 composite, we have shown that it is under sufficient residual stress to significantly distort the unit cell, resulting in a reduced volume equivalent to a much higher compression of 4 GPa. Another issue is the claim that the Raman peak at ~350 cm^{-1}, which is commonly associated with r8-Si, can be attributed instead to bc8-Si [46]. However, Raman peak positions shift with changing pressure, the effect of which has also been measured for Si [48]. Here we have shown that, under a residual stress of 4 GPa, good agreement between the measured peak position and the DFT-calculated peak position is achieved if and only if the peak at ~350 cm^{-1} is attributed to r8-Si. Indeed, there is no indication in the results presented here that a peak observed at ~350 cm^{-1} could be attributed to bc8-Si regardless of pressure, nor would there be sufficient calculated peaks relating to bc8-Si to account for all the experimentally observed peaks. Instead, we suggest that any previously reported experimental observations of a

peak at ~350 cm^{-1} after DAC decompression is due to the presence of residual volumes of r8-Si [6].

In summary, a novel method for performing XRD on material phase transformed via indentation has been presented. XRD data from the recovered bc8/r8 composite material indicate that the composite is predominantly r8-Si, comprising ~70% of the material. It further shows that the structure has a distorted unit cell, with elongation along the indentation axis that results in an overall reduction in the unit cell volume relative to the same phases recovered from DAC compression. This reduction is equivalent to a compression of ~4 GPa in a DAC. This volume reduction is supported by DFT calculations, showing a significant improvement in the fit between the DFT-calculated and experimentally observed Raman peak positions of the bc8/r8 composite. The DFT data also indicate that, at the reduced volume, r8-Si is more energetically favorable than bc8-Si, in agreement with the observation that r8-Si is the predominant phase in the composite material.

The controlled formation of r8-Si presented in this study opens up several avenues for further study. First and foremost is to further explore the electrical and optical properties of the r8-dominant composite material to confirm the desired semiconducting predicted properties [14–16]. Furthermore, understanding the transition pathway and pressure distributions that have resulted in r8-Si remaining stable after complete decompression may lead to other Si phases to be more readily recovered. In particular, the ability to engineer the stress distribution during and after indentation has wider applications, as the results may be applied to a wider range of materials such as C and Ge, as well as possible other industrially relevant semiconductors.

We would like to acknowledge and thank Beamline Scientist Ruqing Xu for his help in obtaining the X-ray data. J. E. B. would like to acknowledge the Australian Research Council (ARC) (FT130101355). B. H. gratefully acknowledges funding through a Weinberg Fellowship sponsored by the Laboratory Directed Research and Development Program of Oak Ridge National Laboratory, managed by UT-Battelle, LLC, for the U.S. Department of Energy and ORNL's Neutron Facilities, a DOE Office of Science User Facility operated by the Oak Ridge National Laboratory. A. M. acknowledges support from MINECO Project No. MAT2016-75586-C4-3-P (Spain). The authors acknowledge the facilities, and the scientific and technical assistance, of the Australian Microscopy and Microanalysis Research Facility at the RMIT Microscopy and Microanalysis Facility, at RMIT University. Portions of this work were performed at XSD-SSM, Advanced Photon Source (APS), Argonne National Laboratory. The Advanced Photon Source is a U.S. Department of Energy (DOE) Office of Science User Facility operated for the DOE Office of Science by Argonne National Laboratory under Award No. DE-AC02-06CH11357

[1] J. E. Bradby, J. S. Williams, J. Wong-Leung, M. V. Swain, and P. Munroe, J. Mater. Res. **16**, 1500 (2001).
[2] J. Z. Hu, L. D. Merkle, C. S. Menoni, and I. L. Spain, Phys. Rev. B **34**, 4679 (1986).
[3] A. Kailer, Y. G. Gogotsi, and K. G. Nickel, J. Appl. Phys. **81**, 3057 (1997).
[4] M. I. McMahon and R. J. Nelmes, Phys. Rev. B **47**, 8337 (1993).
[5] G. M. Pharr, W. C. Oliver, and D. S. Harding, J. Mater. Res. **6**, 1129 (1991).
[6] R. O. Piltz, J. R. Maclean, S. J. Clark, G. J. Ackland, P. D. Hatton, and J. Crain, Phys. Rev. B **52**, 4072 (1995).
[7] A. Mujica, A. Rubio, A. Munoz, and R. J. Needs, Rev. Mod. Phys. **75**, 863 (2003).
[8] M. Beekman, Mater. Today **18**, 304 (2015).
[9] B. Haberl, T. A. Strobel, and J. E. Bradby, Appl. Phys. Rev. **3**, 040808 (2016).
[10] C. Rodl, T. Sander, F. Bechstedt, J. Vidal, P. Olsson, S. Laribi, and J. F. Guillemoles, Phys. Rev. B **92**, 045207 (2015).
[11] P. C. Taylor, Phys. Today **69**, No. 12, 34 (2016).
[12] Q. Q. Wang, B. Xu, J. Sun, H. Y. Liu, Z. S. Zhao, D. L. Yu, C. Z. Fan, and J. L. He, J. Am. Chem. Soc. **136**, 9826 (2014).
[13] S. Wippermann, Y. P. He, M. Voros, and G. Galli, Appl. Phys. Rev. **3**, 040807 (2016).
[14] B. D. Malone, J. D. Sau, and M. L. Cohen, Phys. Rev. B **78**, 035210 (2008).
[15] M. L. Cohen and B. D. Malone, J. Appl. Phys. **109**, 102402 (2011).
[16] B. D. Malone, J. D. Sau, and M. L. Cohen, Phys. Rev. B **78**, 161202 (2008).
[17] S. Minomura and H. G. Drickamer, J. Phys. Chem. Solids **23**, 451 (1962).
[18] R. H. Wentorf and J. S. Kasper, Science **139**, 338 (1963).
[19] V. Domnich, Y. Gogotsi, and S. Dub, Appl. Phys. Lett. **76**, 2214 (2000).
[20] E. R. Weppelmann, J. S. Field, and M. V. Swain, J. Mater. Res. **8**, 830 (1993).
[21] I. Zarudi, L. C. Zhang, W. C. D. Cheong, and T. X. Yu, Acta Mater. **53**, 4795 (2005).
[22] S. Ruffell, K. Sears, A. P. Knights, J. E. Bradby, and J. S. Williams, Phys. Rev. B **83**, 075316 (2011).
[23] D. L. Bish, and J. E. Post, *Modern Powder Diffraction* (Walter de Gruyter GmbH & Co KG, Berlin, 2019), Vol. 20.
[24] S. Wong, B. Haberl, J. S. Williams, and J. E. Bradby, Appl. Phys. Lett. **106**, 252103 (2015).
[25] B. Haberl, J. E. Bradby, S. Ruffell, J. S. Williams, and P. Munroe, J. Appl. Phys. **100**, 013520 (2006).
[26] S. Wong, B. Haberl, J. S. Williams, and J. E. Bradby, J. Appl. Phys. **118**, 245904 (2015).
[27] S. Roorda, W. C. Sinke, J. M. Poate, D. C. Jacobson, S. Dierker, B. S. Dennis, D. J. Eaglesham, F. Spaepen, and P. Fuoss, Phys. Rev. B **44**, 3702 (1991).
[28] S. Wong, B. Haberl, J. S. Williams, and J. E. Bradby, Exp. Mech. **57**, 1037 (2017).
[29] See Supplemental Material at http://link.aps.org/supplemental/10.1103/PhysRevLett.122.105701, for indentation load-unload curve, which includes Refs. [30–32].

[30] J. E. Bradby, J. S. Williams, and M. V. Swain, Phys. Rev. B **67**, 085205 (2003).
[31] L. Chang and L. C. Zhang, Mater. Sci. Eng. A **506**, 125 (2009).
[32] S. Ruffell, J. E. Bradby, J. S. Williams, and P. Munroe, J. Appl. Phys. **102**, 063521 (2007).
[33] B. C. Johnson, B. Haberl, J. E. Bradby, J. C. McCallum, and J. S. Williams, Phys. Rev. B **83**, 235205 (2011).
[34] C. Prescher and V. B. Prakapenka, High Press. Res. **35**, 223 (2015).
[35] B. H. Toby and R. B. Von Dreele, J. Appl. Crystallogr. **46**, 544 (2013).
[36] See Supplemental Material at http://link.aps.org/supplemental/10.1103/PhysRevLett.122.105701, for indentation load-unload curve, which includes Ref. [6].
[37] F. Birch, Phys. Rev. **71**, 809 (1947).
[38] G. Kresse and J. Furthmuller, Comput. Mater. Sci. **6**, 15 (1996).
[39] G. Kresse and J. Hafner, Phys. Rev. B **47**, 558 (1993).
[40] J. P. Perdew, K. Burke, and Y. Wang, Phys. Rev. B **54**, 16533 (1996).
[41] G. Kresse and D. Joubert, Phys. Rev. B **59**, 1758 (1999).
[42] A. Mujica, C. J. Pickard, and R. J. Needs, Phys. Rev. B **91**, 214104 (2015).
[43] A. Kailer, K. G. Nickel, and Y. G. Gogotsi, J. Raman Spectrosc. **30**, 939 (1999).
[44] S. Ruffell, B. Haberl, S. Koenig, J. E. Bradby, and J. S. Williams, J. Appl. Phys. **105**, 093513 (2009).
[45] P. F. McMillan *et al.*, Phase Transitions **80**, 1003 (2007).
[46] M. M. Chaudhri, Phys. Rev. B **84**, 237301 (2011).
[47] E. Bonera, M. Fanciulli, and D. N. Batchelder, Appl. Phys. Lett. **81**, 3377 (2002).
[48] H. Olijnyk and A. P. Jephcoat, Phys. Status Solidi B **211**, 413 (1999).